AGU PUBLICATIONS

JGR

Journal of Geophysical Research: Oceans

RESEARCH ARTICLE

10.1002/2015JC010970

Key Points:
- A two-parameter model based on molecular diffusion and convective sorting only
- The model tested in three natural systems remarkably agrees with field measurements
- Boundary conditions affect the large-scale dynamics of double-diffusive staircases

Correspondence to:
M. Toffolon,
marco.toffolon@unitn.it

Citation:
Toffolon, M., A. Wüest, and T. Sommer (2015), Minimal model for double diffusion and its application to Kivu, Nyos, and Powell Lake, *J. Geophys. Res. Oceans*, *120*, 6202–6224, doi:10.1002/2015JC010970.

Received 13 MAY 2015
Accepted 17 AUG 2015
Accepted article online 21 AUG 2015
Published online 13 SEP 2015

Minimal model for double diffusion and its application to Kivu, Nyos, and Powell Lake

Marco Toffolon[1,2], Alfred Wüest[2,3], and Tobias Sommer[3]

[1]Department of Civil, Environmental and Mechanical Engineering, University of Trento, Trento, Italy, [2]Physics of Aquatic Systems Laboratory, Margaretha Kamprad Chair, École Polytechnique Fédérale de Lausanne, Institute of Environmental Engineering, Lausanne, Switzerland, [3]Eawag, Swiss Federal Institute of Aquatic Science and Technology, Surface Waters - Research and Management, Kastanienbaum, Switzerland

Abstract Double diffusion originates from the markedly different molecular diffusion rates of heat and salt in water, producing staircase structures under favorable conditions. The phenomenon essentially consists of two processes: molecular diffusion across sharp interfaces and convective transport in the gravitationally unstable layers. In this paper, we propose a model that is based on the one-dimensional description of these two processes only, and—by self-organization—is able to reproduce both the large-scale dynamics and the structure of individual layers, while accounting for different boundary conditions. Two parameters characterize the model, describing the time scale for the formation of unstable water parcels and the optimal spatial resolution. Theoretical relationships allow for the identification of the influence of these parameters on the layer structure and on the mass and heat fluxes. The performances of the model are tested for three different lakes (Powell, Kivu, and Nyos), showing a remarkable agreement with actual microstructure measurements.

1. Introduction

Double diffusion is a process resulting from the different rates of molecular diffusion of mass and heat in a fluid, which encompasses a wide range of natural environments [*Turner*, 1974; *Huppert and Turner*, 1981]. Here we focus on what is called the "diffusive regime of double-diffusive convection" [*Turner*, 1965; *Kelley et al.*, 2003]. In this case, a destabilizing temperature profile (i.e., increasing downward when above the temperature of maximum density) is counterbalanced by the stabilizing effect of a downward increase in salinity. If the effect of salinity is stronger than that of temperature, the system is stable with continuous profiles. However, a second dynamically stable configuration exists in some cases, where both temperature and salinity form uniform layers (with convective motions due to local instability) separated by sharp interfaces dominated by molecular diffusion, leading to the formation of a staircase structure. Conversely, the so-called "salt fingers" result from the destabilizing effect of salinity balanced by a stabilizing temperature profile [e.g., *Schmitt*, 1994]. For a deeper introduction on the topic, the reader is referred to the recent book by *Radko* [2013].

Modeling the formation of the organized structures in double-diffusive systems is a complex issue. Different models have been proposed to describe the phenomenon [e.g., *Marmorino and Caldwell*, 1976; *Linden and Shirtcliffe*, 1978; *Newell*, 1984; *Fernando*, 1989; *Kelley*, 1990], covering a wide range of approaches: from relatively simple parameterizations (e.g., recently *Gonzalez-Juez et al.* [2011]; see *Kelley et al.* [2003] for a classical review) to much more complex two-dimensional [e.g., *Noguchi and Niino*, 2010a; *Carpenter and Timmermans*, 2014] or even three-dimensional Direct Numerical Simulations (DNS) in oceanic [e.g., *Carpenter et al.*, 2012a; *Mirouh et al.*, 2012; *Flanagan et al.*, 2013] as well as stellar environments [*Wood et al.*, 2013]. So far, most of these models have focused on the properties of the interfaces between layers, such as their thickness, the heat and mass flux through them, and the characteristic dimensionless ratios. Attempts to determine the conditions for the formation of double-diffusive layers, the layer thickness and their stability [*Huppert*, 1971; *Kelley*, 1984] have been proposed for the diffusive and the salt finger regimes [*Radko*, 2003, 2005], and theoretical considerations have been formulated to explain the layer merging mechanisms [*Radko*, 2007; *Noguchi and Niino*, 2010b; *Radko et al.*, 2014a]. However, coupling local dynamics and large-scale effects in the description of the process by which the typical staircase structure forms and evolves is

still an unresolved task. On the one hand, the theoretical findings developed through conceptual models and stability analyses are not easily applied to real profiles in natural waters considering the staircase dynamics and the large-scale boundary conditions. On the other hand, DNS are not yet able to reproduce real-scale phenomena (i.e., scales larger than a single mixed layer), so that their application is mainly limited to the analysis of individual processes [*Sommer et al*., 2014]. Our attempt is to partially fill this gap by deriving a tool to examine the large-scale evolution and interactions without focusing on the small-scale details of the individual steps.

Here we present most likely the simplest possible model reproducing the layering in double-diffusive systems. It is a mechanistic model because it is based on two clearly identified physical processes: (i) the diffusion of heat and mass and (ii) the convective restratification of instabilities produced by the previous process. No discontinuous structures (with marked variations of the local gradients, as in double-diffusive staircases) can be produced without a balance between those contrasting processes [*Turner*, 1974], and these are the only elements of the model. The two processes are solved numerically, introducing only two model parameters and computing the thermophysical quantities using well-established empirical relationships. The formation of the staircase structures is triggered by small disturbances, which initially give rise to a chaotic process and, eventually, to an ordered configuration through a process of self-organization in uniform layers and interfaces.

The formation of mixed layers and interfaces was previously explained by means of the concept of negative diffusion in the context of a purely diffusive process [e.g., *Radko*, 2013]. Although this kind of model is somehow analogous to that proposed in this paper, the Lagrangian reordering that we use for restratification is a more physically reasonable description. In this respect, the sorting procedure is similar to the triplet map rearrangement proposed by *Kerstein* [1999] in the context of one-dimensional turbulence. Our model may also be seen as a discrete version of the analytical model of *Linden and Shirtcliffe* [1978], which, however, was not designed to reproduce large-scale structures. An extension of this model accounting for the time dependence was proposed by *Worster* [2004].

In order to test the model capabilities, we consider deep lake water columns where turbulent mixing is weak. In particular, we selected three lakes where staircase structures have been observed and measured with high vertical resolution. The first case is Powell Lake, with a clearly visible staircase structure in the deep water [*Osborn*, 1973; *Scheifele et al*., 2014]. The staircase structure of the second case, Lake Kivu, has been intensively studied through the collection of a large number of microstructure (conductivity, temperature, and depth) profiles [*Sommer et al*., 2013]. The last examined case, Lake Nyos, is particularly interesting because the formation dynamics of the typical double-diffusive structure has been observed and temperature and salinity profiles have been measured over some years [*Schmid et al*., 2003, 2004]. Modeling the evolution in this case is challenging because the model has to reproduce the temporal variation and not only the steady state configuration.

The paper is organized as follows. Section 2 introduces the model, while its properties are analyzed in section 3 with an attempt to provide a physical interpretation of the main parameters. The model is then applied to three case studies (section 4) and the performances are discussed in section 5. Final conclusions are drawn in section 6.

2. Formulation of the Model

The main dynamics leading to the formation of staircase structures (see the sketch in Figure 1) in double-diffusive convection is described by means of a one-dimensional model, which is composed of only two processes: (i) vertical diffusion of temperature and salinity and (ii) sorting of gravitationally unstable regions. The idea behind this simplified scheme is the splitting of the diffusive and the convective problem. While the first is treated in a standard Eulerian framework, the second is modeled through a Lagrangian displacement of unstable parcels (for a similar formulation in a completely different context see *Piccolroaz and Toffolon* [2013]). The discretization in water parcels and Eulerian grid points is the same for the two submodels, leading to a simple implementation.

2.1. Diffusion and Resorting

Diffusion is the first process considered. In absence of convective instability, the vertical dynamics of the conservative properties, temperature T and salinity S, are governed by the diffusion equations:

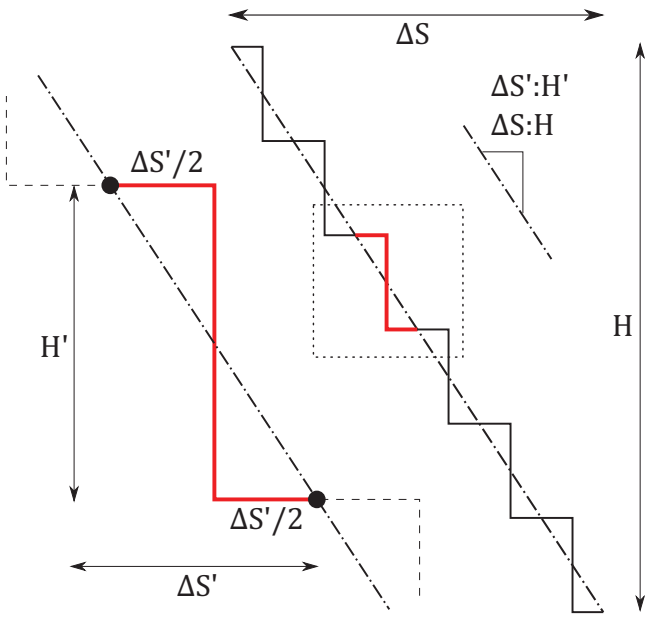

Figure 1. Single step isolated from a series of identical steps along the large-scale profile of salinity. The same picture is valid for temperature.

$$\frac{\partial T}{\partial t}=\kappa_T\frac{\partial^2 T}{\partial z^2}, \qquad \frac{\partial S}{\partial t}=\kappa_S\frac{\partial^2 S}{\partial z^2}, \tag{1}$$

where κ_T and κ_S are the molecular diffusion coefficients. The ratio between the two coefficients,

$$\tau=\frac{\kappa_S}{\kappa_T}, \tag{2}$$

is one of the main parameters characterizing double diffusion. The process of molecular diffusion of salinity is much slower than for temperature and typical ratios are $\tau \simeq 0.01$.

The second process is the vertical sorting of unstable regions. After the solution of the diffusion problems, the density profile is calculated for the whole water column, and the regions that are not in gravitational equilibrium are sorted to have a monotonic increase of density with the depth.

We express water density ρ as a function of temperature T, salinity S, and pressure p. Water density and the other thermophysical quantities are computed using the *Fofonoff and Millard* [1983] equation of state for Powell Lake, and using a parameterization based on the ionic composition of the water [*Wüest et al.*, 1996] for the other two lakes (Nyos and Kivu). As we consider only small density changes due to small variations of T and S, we approximate ρ by the Taylor expansion around temperature T_r and salinity S_r (the subscript r denotes reference values), locally neglecting the influence of pressure. Therefore,

$$\rho(T,S) \simeq \rho_r[1-\alpha(T-T_r)+\beta(S-S_r)], \tag{3}$$

where

$$\rho_r=\rho(T_r,S_r), \quad \alpha=-\frac{1}{\rho_r}\frac{\partial\rho}{\partial T}\bigg|_{T_r}, \quad \beta=\frac{1}{\rho_r}\frac{\partial\rho}{\partial S}\bigg|_{S_r}. \tag{4}$$

The diffusive fluxes for T and S are defined as

$$\phi_T=-\kappa_T\frac{\partial T}{\partial z}, \qquad \phi_S=-\kappa_S\frac{\partial S}{\partial z}, \tag{5}$$

and we will also refer to the heat flux $\phi_H=\rho\, c_p\, \phi_T$, where c_p is the heat capacity of water at constant pressure.

2.2. Double Diffusion Parameters

A few dimensionless numbers can be introduced thanks to the simplified form of equation (3). The "density ratio" characterizes the large-scale variation of temperature and salinity:

$$R_\rho=\frac{\beta\Delta S}{\alpha\Delta T}, \tag{6}$$

where ΔS and ΔT are the differences of the variables along the region considered. Density variation can hence be expressed as

$$\frac{\Delta\rho}{\rho_r}=\beta\Delta S-\alpha\Delta T=\alpha\Delta T\left(R_\rho-1\right), \tag{7}$$

where values of $R_\rho > 1$ indicate a stable configuration ($\Delta\rho > 0$). Double-diffusive staircases typically exist for R_ρ in the range of 1.5–10 [*Kelley et al.*, 2003].

The staircase structure is characterized by relatively large well-mixed layers (with almost uniform T and S) bounded by thin interfaces on either sides. Introducing the difference $\Delta C'$ across this interfaces, where C generically stands for T or S and the prime is used for the variables that are defined for a single step, we can define the following estimate for the interface thickness:

$$h_C = -\Delta C' \left(\frac{\partial C}{\partial z}\right)^{-1} = \frac{\kappa_C \Delta C'}{\phi_C} . \tag{8}$$

The "density flux ratio" is defined as

$$R_F = \frac{\beta\, \phi_S}{\alpha\, \phi_T} . \tag{9}$$

Across a diffusive interface of thickness h_T (for temperature) and h_S (for salinity), defined according to equation (8), this ratio can be calculated as

$$R'_F = \tau\, r\, \frac{\beta\, \Delta S'}{\alpha\, \Delta T'} , \tag{10}$$

where $r = h_T / h_S$ is the interface thickness ratio. It follows that the density flux ratio can also be rewritten as $R'_F = R'_\rho\, \tau\, r$ [e.g., *Sommer et al.*, 2013], where R'_ρ is defined by equation (6) using the differences across the step.

2.3. Numerical Solution and Model Parameters

The one-dimensional equations (1) are solved numerically with the proper boundary conditions, as described in Appendix A, either in the Dirichlet (i.e., imposing the values of the variables) or Neumann (imposing the fluxes) form.

Given the Lagrangian algorithm for stabilization, the discrete structure is an inherent characteristic of the model. The computational domain, having height L, is divided into $n+1$ points with a grid size $dz = L/n$. The numerical solution of the diffusion equation introduces a second (this time dimensionless) parameter of the model,

$$\lambda_T = \frac{\kappa_T\, dt}{dz^2} , \tag{11}$$

which relates the time step dt and the grid size dz. An implicit scheme is adopted for the numerical solution, such that the algorithm is always stable without conditions on λ_T.

An example of the effect of λ_T on the formation of a gravitationally unstable volume of water (i.e., with upward increasing ρ, possibly leading to convective instability) is provided in Figure 2. The profiles of T and S are plotted after one time step dt starting from the same initial condition, in a case in which a simple analytical solution exists:

$$C(z, dt) = C_0 + \frac{\Delta C'}{2}\left[1 - \mathrm{erf}\left(\frac{z}{\sqrt{4\,\kappa_C\, dt}}\right)\right] , \tag{12}$$

with C_0 the constant value of the variable (T or S) in the mixed layer and $\Delta C'$ the interface step. Having fixed the grid size dz, the time step (during which T and S diffuse) changes with λ_T according to the definition (11). It is clear that larger values of λ_T tend to create a larger number of water parcels that effectively contribute to the reorder operated by the sorting algorithm to reestablish the stability of the system.

3. Interpretation of Model Parameters

The model contains only two parameters that require calibration: dz and λ_T. The former represents the volume of the individual water parcels that are displaced by convection; the latter is a dimensionless time step over which the diffusion process acts before triggering instability. Consistent with the adopted Lagrangian approach, dz is not a merely computational parameter but contains information about the system to be described. As similar considerations hold for λ_T, we first analyze a simplified setup of the model to grasp the role of these parameters.

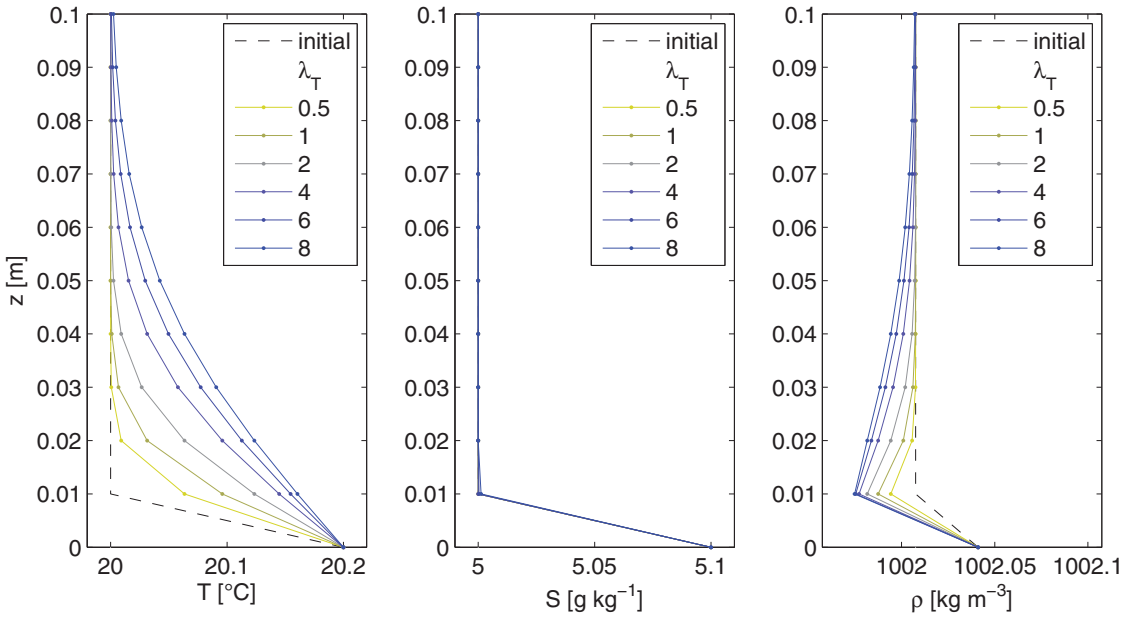

Figure 2. Analytical curves obtained after one numerical time step $dt=\lambda_T dz^2/\kappa_T$ for different values of λ_T (see legend) starting from a Heaviside function, for $dz=0.01$ m. Density is calculated using equation (3) with $\alpha=2.1\times10^{-4}$ °C^{-1}, $\beta=7.5\times10^{-4}$ kg g^{-1}, and $\rho_r=1002.0$ kg m^{-3} ($T_r=20$°C, $S_r=5$ g kg^{-1}).

3.1. The Model for a Single Step

We consider a single step characterized by a height H' (using again the prime $'$ to denote quantities referred to the step) and difference of temperature $\Delta T'$ and salinity $\Delta S'$ (see Figure 1). Accordingly, we define the density ratio (6) for the step as

$$R_\rho' = \frac{\beta\,\Delta S'}{\alpha\,\Delta T'}\,. \tag{13}$$

In this analysis, we assume that the large-scale profile (characterized by a staircase structure over a height H) contains a large number of steps, so that the slope of the large-scale profiles ($\Delta S/H$, $\Delta T/H$) is a good approximation of an individual step ($\Delta S'/H'$, $\Delta T'/H'$). Thus, it directly follows that $R_\rho \simeq R_\rho'$.

We assume that a dynamic steady state has been reached, whereby the diffusive flux across the interface is balanced by the flux through the convective layer: two phases alternate with the creation of a gravitationally unstable boundary layer (by diffusion) and its destruction (by convection). Figure 3 qualitatively illustrates typical profiles of temperature, salinity, and density after the two phases of the model (i.e., solution of the diffusion equation and sorting of unstable regions).

The balance requires the quantification of the diffusive ($\phi_{T,diff}$ and $\phi_{S,diff}$) and convective ($\phi_{T,conv}$ and $\phi_{S,conv}$) fluxes. Section B1 tackles this problem and provides the derivation of the steady state fluxes. The calculation of the diffusive fluxes is straightforward from a numerical point of view, while the convective fluxes can be computed by counting the number of gravitationally unstable Lagrangian water parcels that are transported in each time step dt. By defining n_u parcels of size dz on each side of the step and assuming a symmetrical shape, we can express the convective flux as

$$\phi_{C,conv} = 2\sum_{i=1}^{n_u}\frac{(C_i-C_r)\,dz}{dt} = 2\,m_C\,\frac{(C_1-C_r)\,dz}{dt}\,, \tag{14}$$

where C again stands for T or S, the subscript r indicates the reference conditions for the step, and the coefficients,

$$m_T = \frac{1+\sqrt{1+2\lambda_T}}{2}\,, \qquad m_S = \frac{1+\sqrt{1+2\lambda_S}}{2}\,, \tag{15}$$

quantify the dimensionless transported "mass," as demonstrated in section B2. The number n_u of cells affected by the convective motion is plotted in Figure 4a as a function of λ_T, along with m_T and m_S in Figure 4b (assuming two different values of τ to calculate $\lambda_S=\kappa_S\,dt/dz^2$).

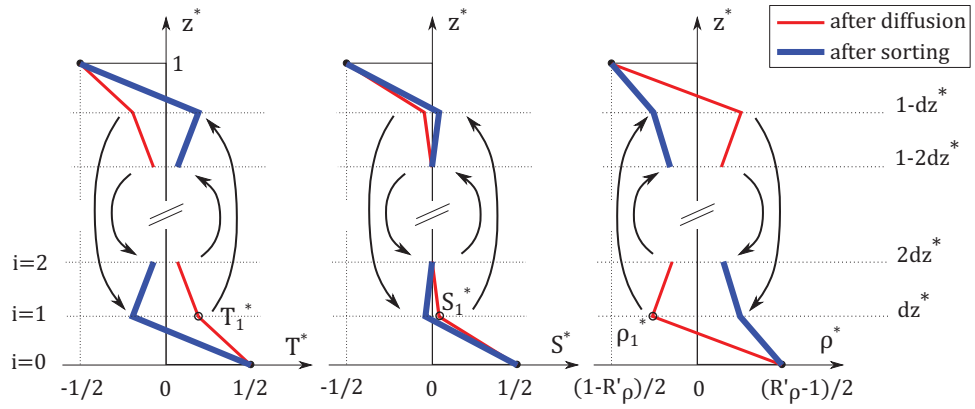

Figure 3. A sketch of the process of diffusion and resorting of temperature and salinity, with their influences on density, in a single step in conditions of dynamic equilibrium. The profiles are plotted after the solution of the diffusion equation (thin red lines) and after the reordering of the unstable region (thick blue lines; arrows represent the Lagrangian displacement during sorting).

By satisfying the balance between diffusion and convection, we obtain (see Appendix B) that

$$\phi_T = \frac{\kappa_T \, \Delta T'}{dz \, \eta_T}, \qquad \phi_S = \frac{\kappa_S \, \Delta S'}{dz \, \eta_S} \tag{16}$$

with

$$\eta_T = 2 + \frac{\lambda_T}{m_T} = 2m_T, \qquad \eta_S = 2 + \frac{\lambda_S}{m_S} = 2m_S \, . \tag{17}$$

We note that $\eta_S \simeq 2$ if $\lambda_S \ll 2m_S$. Exploiting the relationships (15) and (17), it can be derived that such a condition implies $\lambda_S \ll 4$, or equivalently $\lambda_T \ll 4\,\tau^{-1}$, which is usually satisfied given the small value of τ. This condition is used in all the final approximations of the following equations.

It is straightforward to calculate the interface thicknesses according to the definition (8),

$$h_T = \frac{\kappa_T \, \Delta T'}{\phi_T} = dz \, \eta_T \, , \qquad h_S = \frac{\kappa_S \, \Delta S'}{\phi_S} = dz \, \eta_S \, , \tag{18}$$

the interface thickness ratio $r = \eta_T / \eta_S \simeq m_T$, and the density flux ratio,

$$R'_F = R'_\rho \, \tau \, \frac{\eta_T}{\eta_S} \simeq R'_\rho \, \tau \, m_T \, . \tag{19}$$

Eventually, a condition for the existence of the step is derived in Appendix C. For the values of λ_T found for the cases examined in section 4 (from 4 to 7, see Table 1), the condition requires R_ρ to be larger than 1.5–1.6 to have a stable step. Interestingly, these values are very close to the critical value 1.7 for the staircase to form [*Radko et al.*, 2014b], and consistent with observations in the field (e.g., Lake Nyos).

3.2. Breakdown of the Boundary Layer

The identification of a critical Rayleigh number $Ra_c \sim O(10^3)$ for the breakdown of the boundary layer (which implicitly defines the time scale of our problem) was proposed by *Linden and Shirtcliffe* [1978]. In our notation and using h_T as the thickness of the boundary layer, the Rayleigh number reads

$$Ra = \frac{g \, \alpha \, \Delta T' \, h_T^3}{\nu \, \kappa_T} \, , \tag{20}$$

where ν is the kinematic viscosity of water (the value $\nu \simeq 10^{-6}$ m^2 s^{-1} will be used as representative for the following applications) and g is the gravitational acceleration. By requiring $Ra = Ra_c$, we can estimate the value of η_T as follows:

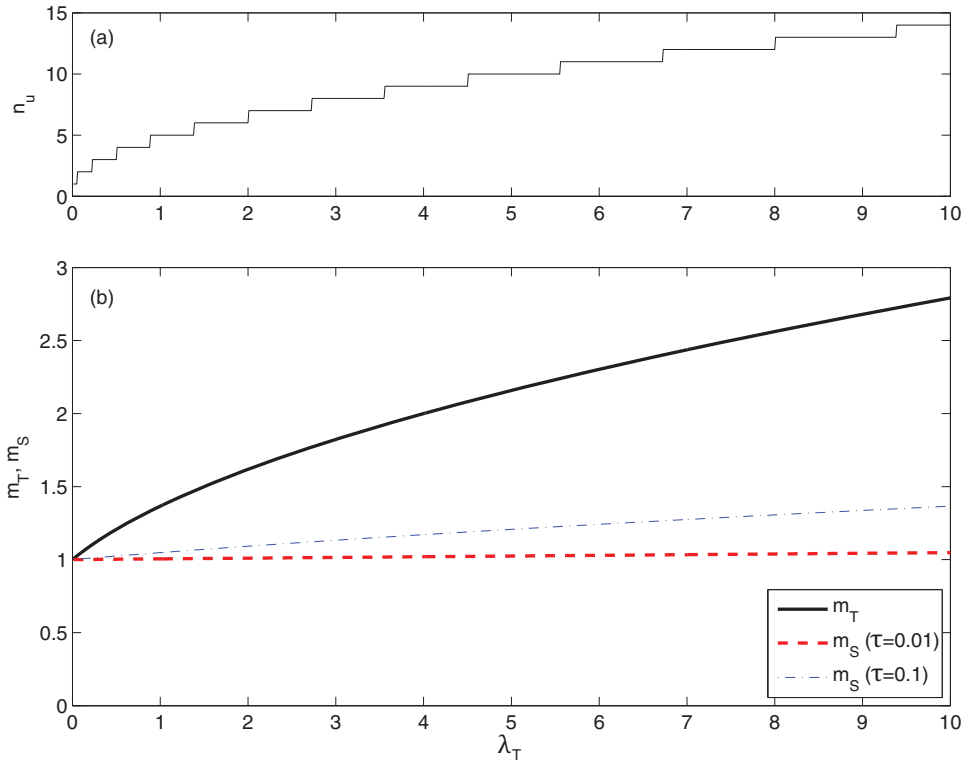

Figure 4. Curves obtained by the theoretical steady state relationships derived in section 3 for a single layer, as a function of λ_T: (a) number n_u of moving cells (assuming $n_\sigma = 3$); (b) relative "mass" m_T and m_S transported for temperature and salinity (assuming two different values of τ), respectively.

$$\eta_T = \left(\frac{\nu \, \kappa_T}{g \, \alpha} \frac{Ra_c}{\Delta T'} \right)^{1/3} dz^{-1} , \tag{21}$$

and consequently the corresponding value of λ_T according to equation (17) (see also Figure 4e). This relationship represents the connection between the numerical (discrete) description of the model and the actual physics. However, it cannot be used as a predictive tool to determine the model parameter λ_T for at least two different reasons. First, the value of Ra_c is still under debate [*Worster*, 2004; *Carpenter et al.*, 2012a]. Second, this relationship includes the step temperature difference $\Delta T'$, which is a result of the process. Notwithstanding these limitations, equation (21) provides a way to validate the calibration of the parameters based on the comparison of the model results with the available measurements that will be performed in section 4.

We can also rewrite equation (21) highlighting the dependence of the interface thickness on the temperature difference, $h_T \propto \Delta T'^{-1/3}$. Substituting this dependence into the flux (16) yields $\phi_T \propto \Delta T'^{4/3}$, which recalls the well-known 4/3 law for the double-diffusive flux [*Kelley et al.*, 2003]. It then follows that the temperature step increases with the flux less than linearly:

Table 1. Model Parameters and Reference Values

Lake	λ_T	dz (m)	L (m)	H (m)	T_r (°C)	S_r (g kg^{-1})	ρ_r (kg m^{-3})	α (°C^{-1})	β (g^{-1} kg)
Test	0.5–8	0.005–0.02	10	8	10	10	1007.5	1.10×10^{-4}	7.71×10^{-4}
Powell	7	0.01	28.3	22	9.3	16.6	1014.3	1.25×10^{-4}	7.65×10^{-4}
Kivu	4	0.01	48.0	30	23.6	2.74	1000.3	2.45×10^{-4}	7.49×10^{-4}
Nyos	4	0.02	48.0	variable in time	22.6	1.69[a]	999.2	2.31×10^{-4}	7.52×10^{-4}

[a]Value of equivalent salinity S_e including the effect of CO_2, whose average concentration in the domain is 66.3 mmol kg^{-1}, with β_{CO_2} = 0.0125 kg mol^{-1} [*Schmid et al.*, 2004]. The reference value of the actual salinity is $S = 0.68$ g kg^{-1}.

$$\Delta T' = \gamma\, \phi_T^{3/4}\,, \qquad \gamma = \left(\frac{\nu\, Ra_c}{g\, \alpha\, \kappa_T^2}\right)^{1/4}\,, \tag{22}$$

where $\gamma \sim 3\times10^3$ $K^{1/4}$ $s^{3/4}$ $m^{-3/4}$ (due to the small exponent, the value of γ does not change by orders of magnitudes in a physically meaningful range of the parameters, apart from the case of vanishing α close to the temperature of maximum density, when however double diffusion does not occur). Given the approximations introduced and the uncertainty in the estimation of Ra_c, the relationship (22) cannot be used to infer the exact value of the temperature steps but provides some hints about the dependence on the main factors.

The above relationships suggest that λ_T should inversely depend (although weakly, given the small exponent) on the flux ϕ_T,

$$\eta_T = \gamma\, \kappa_T\, \phi_T^{-1/4}\, dz^{-1}\,, \tag{23}$$

thus implying that it cannot be considered a constant parameter. This means that the model parameters are likely not general and should be calibrated for the different cases as will be discussed in section 4. Such a need seems to generate an element of circularity in the model: the parameters depend on the heat flux, but at the same time they determine the structure of the staircase, and hence the actual flux that passes through it. However, the circularity is not actually present because the heat flux controls only the interface, while the system adapts to the large-scale boundary conditions by changing the slope of the staircase region, as it is discussed in the following section.

3.3. Interaction With Large-Scale Profiles

In order to understand how the double-diffusive fluxes affect the large-scale profiles of temperature and salinity, we set up a simplified configuration where the initial conditions divide the computational domain (height L) into three regions as shown in Figures 5c and 5d: the central part (height H) is the region where the staircase structure potentially forms, while the fluxes in the boundary regions (each of height δl) are maintained at the level of molecular diffusion by imposing a strong (thus stabilizing) salinity gradient.

The double-diffusive fluxes in the central region can be expressed using the large-scale variables as follows:

$$\phi_T = \kappa_T \frac{\Delta T}{H} \phi_T^*\,, \qquad \phi_S = \kappa_S \frac{\Delta S}{H} \phi_S^*\,, \tag{24}$$

where we assume a large number of identical steps as in Figure 1. The dimensionless fluxes $\phi_T^* = n'/\eta_T$ and $\phi_S^* = n'/\eta_S$ are the ratios of the actual transport with respect to the large-scale purely diffusive fluxes ($n' = H'/dz$ being the number of numerical points in a single step, and recalling that $h_T = \eta_T dz$ and $h_S = \eta_S dz$; see also Appendix B). Noting that η_T and η_S are $\sim O(1)$ and $n' \gg 1$ as a result of the process, we can infer that the double-diffusive convection actually increases the vertical transport with respect to the large-scale diffusive fluxes, a result that is well known in literature [e.g., *Turner*, 1965].

Since salinity is not transported efficiently compared to temperature ($\kappa_S \ll \kappa_T$), we focus on a medium-term analysis for which the temperature flux adapts to the boundary conditions and becomes approximately constant and uniform throughout the entire domain, while the salinity profile is not significantly affected. The average slope of S remains relatively stable over this time scale, and independent of the boundary regions, so we can directly calculate the salinity flux:

$$\phi_S = \kappa_S \frac{\Delta S}{H} \frac{H'}{dz\, \eta_S} \simeq \kappa_S \frac{\Delta S}{H} \frac{H'}{2dz}\,, \tag{25}$$

where the approximation holds for small λ_S.

The temperature profile adapts more rapidly, and its slope changes in time. In this analysis, the boundary conditions for T are fixed imposing a total temperature difference $T_L = \Delta T + 2\,\delta T$ over $L = H + 2\,\delta l$ (see Figures 5c and 5d). The flux in the two boundary layers is due to molecular diffusion, and at equilibrium it must balance the flux in the central region:

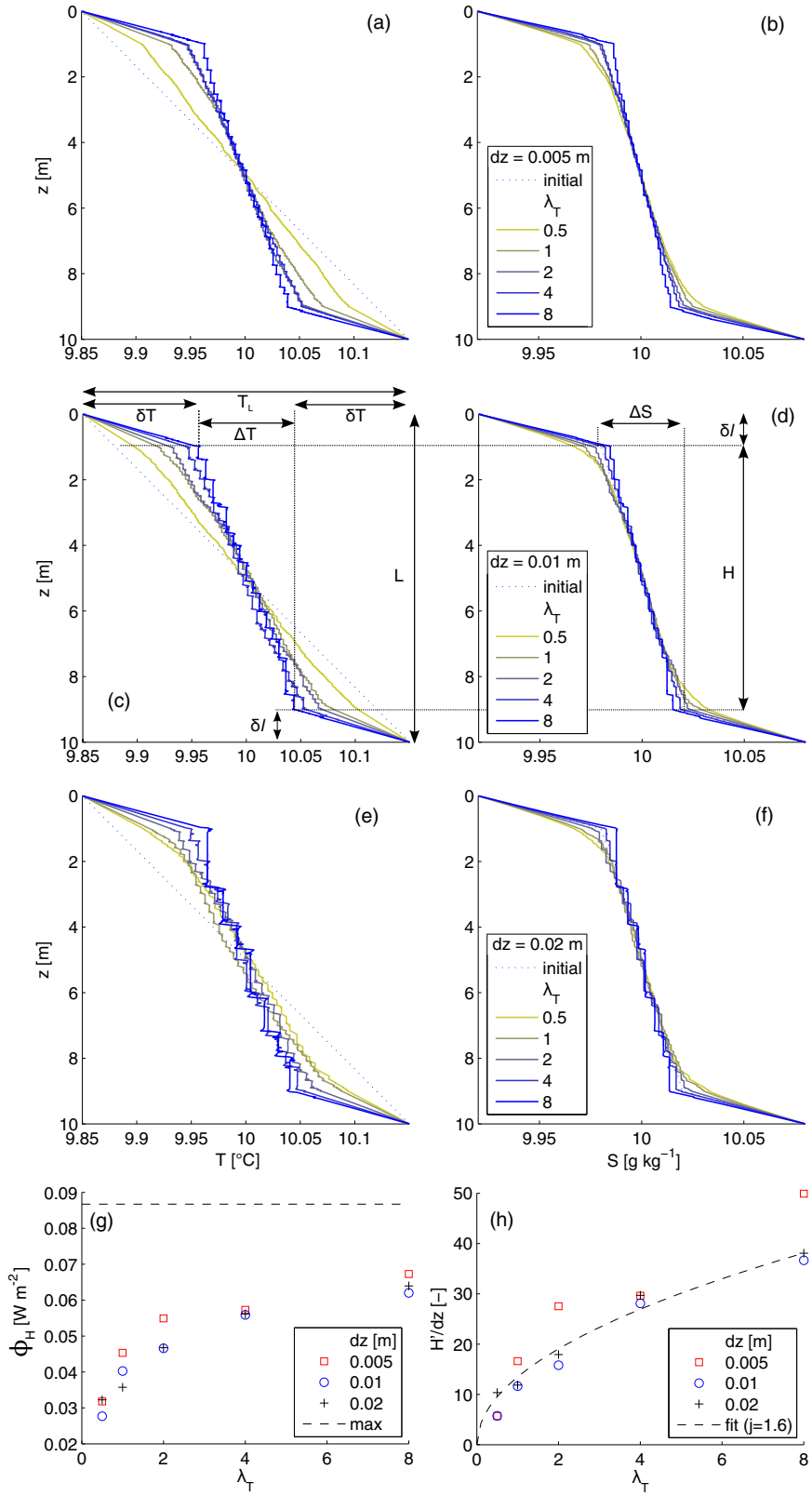

Figure 5. Profiles of (left column) temperature and (right column) salinity in a test case for different values of λ_T (indicated in the legend) and dz: (a, b) $dz = 0.005$ m; (c, d) $dz = 0.01$ m; (e, f) $dz = 0.02$ m. Subplots (Figure 5c) and (Figure 5d) illustrate the definition of the variables used in the main text. Subplots (g, h) show the heat flux ϕ_H and the ratio H'/dz (the dashed line shows the fitting curve proposed in Appendix C using $j = 1.6$), respectively, for the different cases as a function of λ_T.

$$\phi_T = \kappa_T \frac{\delta T}{\delta l} = \kappa_T \frac{\Delta T}{H} \frac{H'}{dz\,\eta_T}\,, \tag{26}$$

which yields a relationship between ΔT and the height H' of the individual steps:

$$\Delta T = T_L \left[1 + \left(\frac{L}{H} - 1\right) \frac{H'}{h_T}\right]^{-1}. \tag{27}$$

With this result, the total flux can be estimated from equation (26):

$$\phi_T = \kappa_T T_L \left[(L-H) + H\,\frac{h_T}{H'}\right]^{-1}. \tag{28}$$

Hence, the ratio H'/h_T of step height to interface thickness appears as a crucial factor to estimate the fluxes in double-diffusive convection. From equations (27) and (28), we see that an increase of such a ratio determines a reduction of ΔT, which implies a steeper staircase, and a larger flux. An exact estimate of the layer height H' is not possible; however, the approximate derivation provided in Appendix C suggests that H' should vary as $\lambda_T^{1/2}$, and linearly with dz. Thus, recalling equation (18), it directly follows that the ratio H'/h_T does not depend on dz but is proportional to $\lambda_T^{1/2}/(2\,m_T) = \lambda_T^{1/2}/\left(1+\sqrt{1+2\lambda_T}\right)$, which rapidly grows with λ_T for small values of the parameter, while it reaches about 80% of the asymptotic value for $\lambda_T \simeq 10$.

These theoretical results are confirmed by a set of simulations performed with the numerical model (Figure 5), where the slope of the temperature profile in the staircase region is analyzed for different values of λ_T (0.5, 1, 2, 4, 8) and dz (0.005, 0.01, 0.02 m). Subplots (a–f) show the profiles obtained after 2000 days, in a condition of approximate steady state. The general tendency is that the temperature profile steepens with λ_T (resulting in a higher flux ϕ_T), while dz has a clear effect only on the step height (we expect that $H' \propto dz$). Indeed, the heat flux ϕ_H grows with λ_T until reaching an asymptotic value (Figure 5g), and $H'/dz \simeq 13.6\,\lambda_T^{1/2}$ (Figure 5h; see also Appendix C), with H' estimated by equation (27).

4. Results

In the following sections, we apply the model to three lakes where detailed measurements are available. In the absence of more accurate information, we assume constant values for the diffusion coefficients: $\kappa_T = 1.4 \times 10^{-7}$ m^2 s^{-1} and $\kappa_S = 1.4 \times 10^{-9}$ m^2 s^{-1}, hence a ratio $\tau = 0.01$. Calibration of the two parameters of the model (dz and λ_T) is performed by visually comparing the results of the numerical simulation with the available measurements.

The boundary conditions are applied in different ways for the three cases because of the different environmental conditions. We note that the choice of suitable boundary conditions (and of the initial condition, especially for the salinity profile) is crucial for the results of the simulation. However, the choice is not simple because the actual boundaries of a homogeneous region are often determined by different processes, like for instance the turbulent mixing in the bottom boundary layer and where lateral intrusions are present. These processes are not included in the model, so the boundary conditions have been adapted to approximately reproduce the same effects by fixing the heat and salt fluxes or the values of temperature and salinity.

4.1. Powell Lake

The first case that we analyze is the deep waters of Powell Lake. Powell Lake (maximum depth $\sim$ 355 m, surface area 90 km^2) is a former fjord in British Columbia, Canada, that got disconnected from the ocean after the last ice-age around 11,000 years ago by continental uplift [*Williams et al.*, 1961; *Scheifele et al.*, 2014]. The relic salty deep water causes a stable stratification. The destabilizing effect of the geothermally heated bottom waters leads to favorable conditions for double diffusion below 290 m depth. Being sheltered from wind by nearby mountains and due to the absence of underwater inflows, the deep water of Powell Lake is extremely calm, which makes it a perfect natural laboratory to study double diffusion.

The model is applied to the depth range between 326 and 355 m, with the staircase structure forming between approximately 330 and 352 m. The upper boundary conditions are imposed by fixing the values of T and S as measured at the top of the investigated domain, which falls within the region of stable gradient

dominated by molecular diffusion. Conversely, the lower boundary condition is imposed by arbitrarily fixing the values of T and S that allow for the existence of another stable region with molecular diffusion. This choice replaces the actual bottom profiles that are almost homogeneous close to the sediment layer, where the bottom boundary mixing is due to a process that is not included in the model.

The initial condition for the salinity profile is chosen such as to resemble the measured profile. The initial temperature profile is chosen to be a linear profile, completely uncorrelated with the measured one. At the beginning of the simulation, a random perturbation is applied to the entire profiles of the order of 10^{-3} °C for temperature and 10^{-4} g kg^{-1} for salinity.

The simulation is run for 10,000 days (~27 years). After such a period, the temperature profile appears to be in a dynamic equilibrium, although it cannot be completely stable due to the slow modification of the salinity profile. In this respect, it is important to note that the model is able to capture the medium-term dynamics (for which salinity is approximately constant), while the long-term variations can be reproduced only by accounting for all the processes and boundary conditions that are responsible for the large-scale vertical structure of the system.

The comparison among the results of the calibrated model and the available measurements [*Scheifele et al.*, 2014] are shown in Figure 6. The values of the parameters λ_T and dz are reported in Table 1, together with the total height of the domain (L), the approximate height of the staircase structure (H) and the approximate reference values (averaged over the domain) of temperature T_r, salinity S_r, density ρ_r, and of the thermophysical parameters α and β. The model is able to reproduce the formation of the staircase structure in an excellent way, with only a small deviation from the measurements of the salinity profile in the region between 330 and 332 m (Figure 6b). The number and height of the step is also well reproduced (Figures 6c and 6d). The small spikes that can be noted in Figure 6c (model results shown after the sorting phase) are due to the convective transport across the two sides of the layers, which is based on reordering the density profile, and disappear after the diffusion phase of the computation.

Figure 7 gives some hints about the type of evolution that leads to such a result. Subplots 7a and 7b show the change of the profiles of T and S, respectively, with time. The salinity profile remains approximately stable. On the contrary, fast and strong changes occur to the temperature profile in the initial phase, when the staircase starts forming and the steps subsequently increase their size (by merging) until reaching an equilibrium value. The vertical flux increases and the temperature difference over the double-diffusive region decreases, as predicted by equations (27) and (28). The other subplots of Figure 7 show the variation of R_ρ (calculated considering the slope over the whole staircase structure) and R_F, and of the interface ratio r, which are all in reasonable agreement with the measurements provided by *Scheifele et al.* [2014]. The resulting heat flux ($\phi_H \simeq 20$ mW m^{-2}) is also close to what is measured (~27 mW m^{-2}) and consistent with the selected temperature profile at the boundaries of the model domain. It is interesting to note that the flux shows a strong increase at the beginning of the simulation when the staircase structure starts forming and the steps grow, while the flux later decreases to the asymptotic equilibrium value because of the reduction of the temperature difference ΔT over the double-diffusive region.

Finally, it is worth verifying whether the calibrated values of the parameters agree with the relationship (21). By referring to the parameters reported in Table 1, estimating a characteristic value of $\Delta T' \simeq 4$ mK in the central part of the staircase, we obtain η_T as a function of Ra_c. If we consider the value $\eta_T \simeq 4.9$ that can be calculated from the calibrated parameter $\lambda_T = 7$, the exact agreement would correspond to a value of the critical Rayleigh number $Ra_c \simeq 5000$, which is in the physically meaningful range of values [*Linden and Shirtcliffe*, 1978; *Carpenter et al.*, 2012a]. We will use this value in the analysis of Lake Kivu as well.

4.2. Lake Kivu

Lake Kivu (maximum depth 485 m, surface area 2370 km^2) is situated in Central Africa between the two countries Rwanda and the Democratic Republic of the Congo and is known for containing large quantities of dissolved methane and carbon dioxide in its deep water. Below 60 m depth, Lake Kivu is permanently stratified. Approximately 78% of the stabilization is caused by salts and 22% percent by the dissolved gases [*Descy et al.*, 2012]. The destabilizing temperature increase toward the sediment is caused by geothermal heating and various warm subaquatic springs. Lake Kivu is an ideal system for studying double diffusion with approximately 300 well-mixed layers distributed almost throughout the entire water column [*Newman*, 1976; *Schmid et al.*, 2010; *Sommer et al.*, 2013].

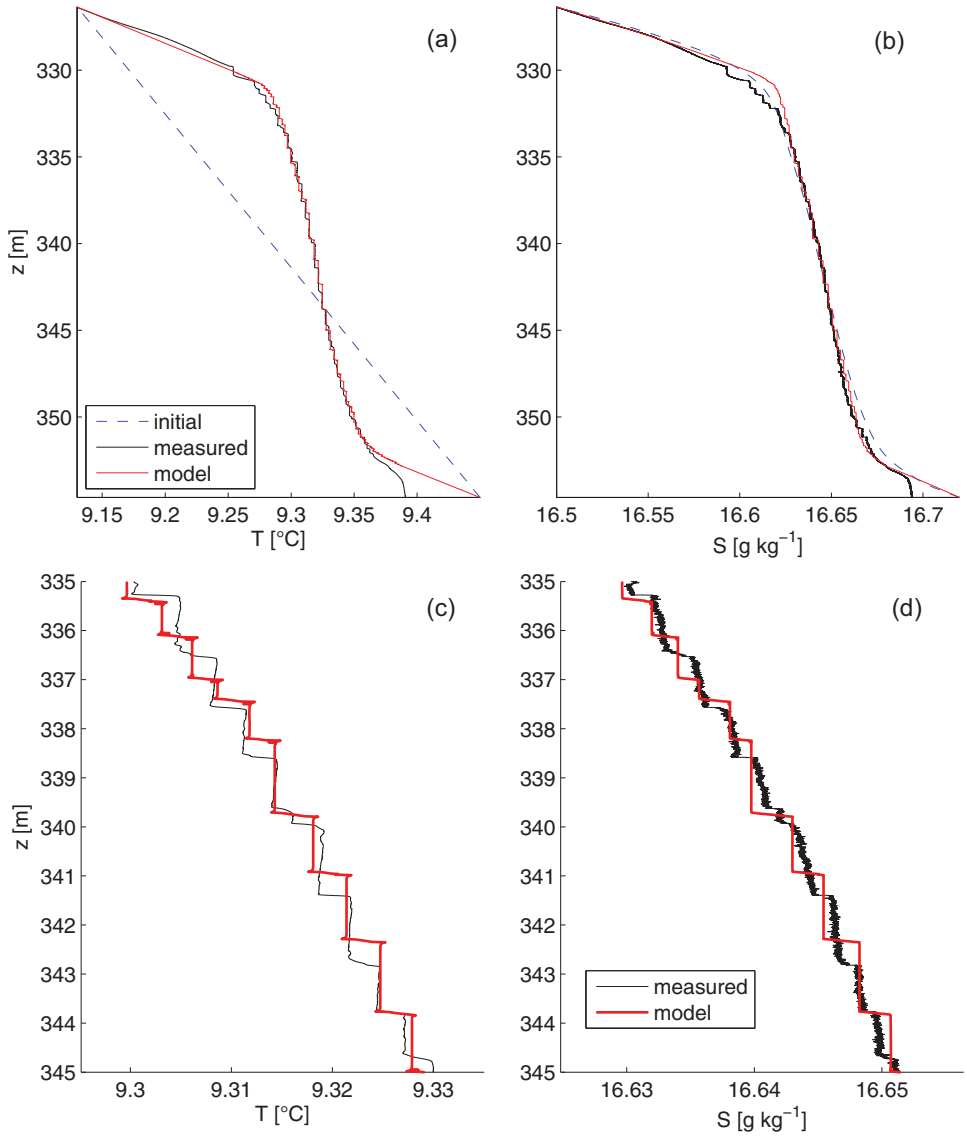

Figure 6. Profiles of (a) temperature and (b) salinity in Powell Lake: comparison among measurements and the results of the model (after sorting), considering a simulation of 10,000 days (~27 years). A zoom over a reach of 10 m is shown in (c) and (d). Model parameters are reported in Table 1.

The model has been applied in the depth range between 161 and 209 m, where a well-defined staircase structure is visible. The initial condition for salinity has been imposed by smoothing the large-scale profile, removing the structure of the steps to avoid the inheritance of the initial condition on the expected staircase. The sigmoidal profile (due to subaquatic sources) has been kept because the transport of salt occurs on a very long time scale. The two boundary conditions have been imposed by fixing the values of S in the first and last grid points in such a way as to have a stable boundary layer with molecular diffusion, which is useful to control the boundary conditions and does not affect the overall results. The initial temperature profile has been chosen arbitrarily with an "erf" shape, and the boundary conditions have been applied in this case by fixing the heat flux. The imposed value is the same (ϕ_H=100 mW m^{-2}) at the upper and lower boundary of the domain [*Sommer et al.*, 2013].

The numerical model is able to simulate an overall picture that significantly agrees with the collected data (Figure 8). The temperature profile evolves and adapts to the measurements at the large scale, and the step structure that spontaneously forms in the central part of the profile for both T and S is very similar to the actual data. Figures 9a and 9b show the total fluxes calculated by means of a mass balance between two

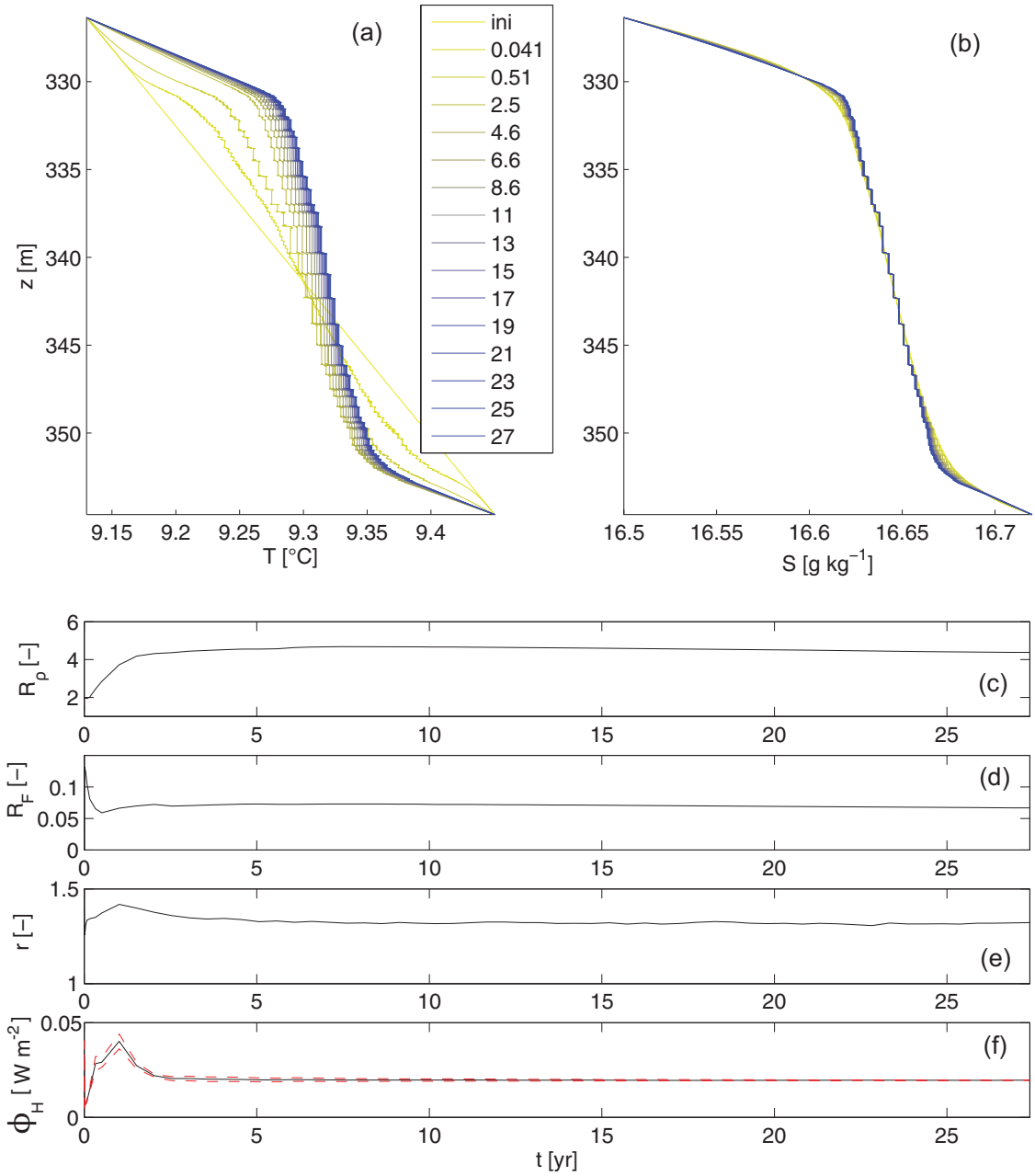

Figure 7. Modeled evolution of (a) temperature and (b) salinity profiles in Powell Lake starting from the chosen initial condition (the legend indicates time in years). Temporal evolution of the averaged parameters: (c) density ratio R_ρ, computed considering the slope of the central part of the profile; (d) flux ratio R_F, computed using the ratio of the mean fluxes; (e) interface ratio r; and (f) heat flux ϕ_H (the dashed lines representing ± one standard deviation of the values along the averaged reach).

time steps. The results suggest that the total heat flux is substantially uniform, while the salt flux is not in a steady state yet. In this respect, we note that reaching an equilibrium for salinity would require much longer simulations that are inevitably affected by the problem of setting realistic boundary conditions. The vertical distribution of the interfaces (Figure 9c) shows a concentration in the central part where the profiles are less steep. Moreover, the range of values of the interface thicknesses for both the temperature and salinity profiles falls within the distributions of the corresponding measurements, as illustrated in Figures 9d–9g.

The parameter values λ_T and dz corresponding to the simulation shown in Figure 8 do not differ much from those used for Powell Lake (Table 1), but the differences are significant. In fact, similarly to the analysis done for Powell Lake, we can test equation (21) also in this case, where the temperature difference across the steps is $\Delta T' \simeq 11$ mK. By assuming the same value $Ra_c \simeq 5000$ used in the previous case, we obtain $\eta_T \simeq 3$.

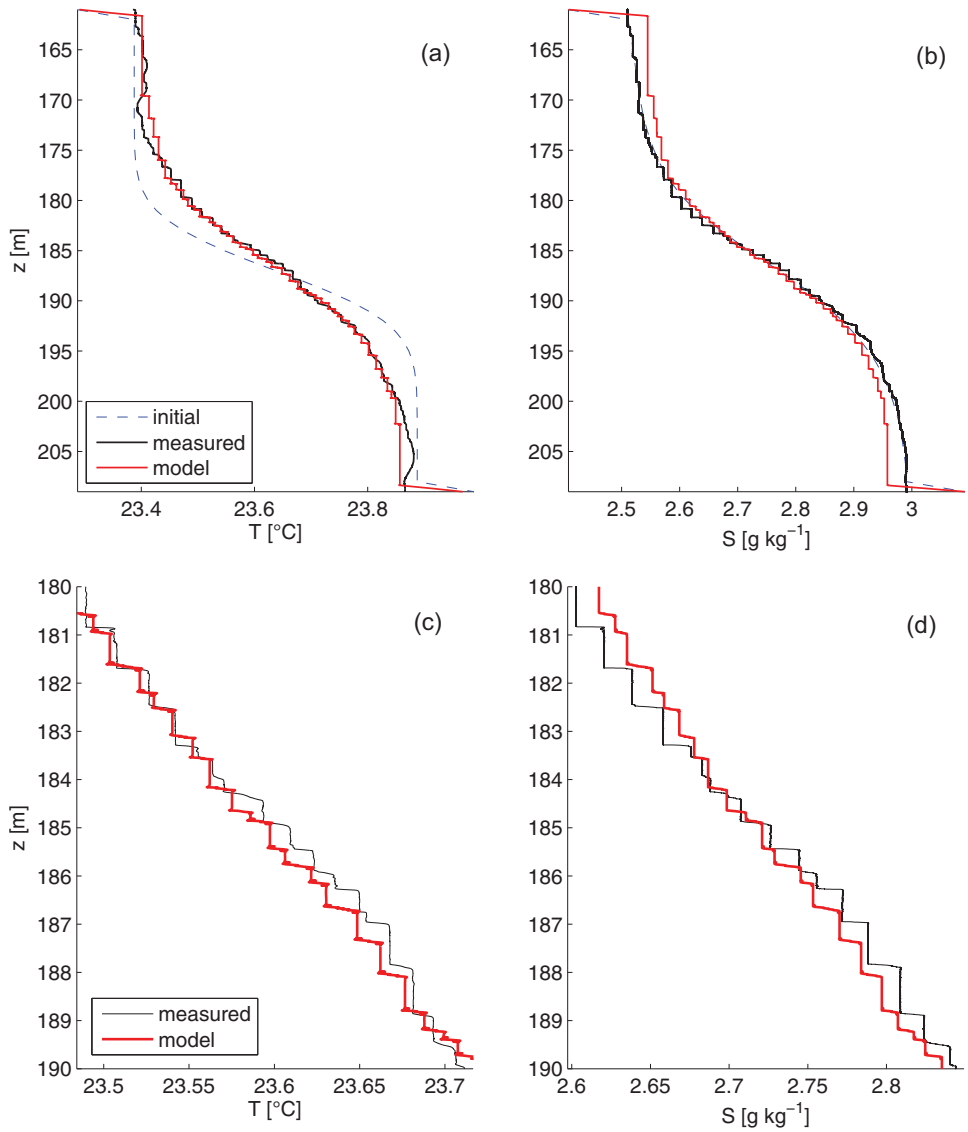

Figure 8. Profiles of (a) temperature and (b) salinity in Lake Kivu: comparison among measurements and the results of the model (after sorting), considering a simulation of 30,000 days (∼82 years). A zoom over a reach of 10 m is shown in (c) and (d). Model parameters are reported in Table 1.

Such a value agrees well with $\eta_T \simeq 4$ that follows from the calibrated value $\lambda_T = 4$. We note that satisfactory results (i.e., producing an agreement between the modeled staircase structure and measurements) could be obtained also by using lower values of λ_T (starting from ∼2), further confirming that the condition (21) is meaningful. Hence, the lower value of λ_T in Lake Kivu with respect to Powell Lake is mainly related to the larger temperature steps in this lake.

We can also use equation (22) to interpret the increase of the temperature steps $\Delta T'$ with the increase of the imposed heat flux ϕ_H and compare the response to the higher heat flux in Lake Kivu relative to Powell Lake. Despite the estimate of $\Delta T'$ from that equation is about half of the measured value (in both cases), the ratio of the temperature steps in Lake Kivu and Powell Lake is $\simeq 2.7$, which is almost exactly confirmed by using the ratio of the fluxes in the right hand side of equation (22).

4.3. Lake Nyos

Lake Nyos is a deep crater lake (maximum depth 208 m, surface area 1.58 km^2) located in the north-western part of Cameroon. The deep waters are separated by a chemocline at ∼53 m depth from the

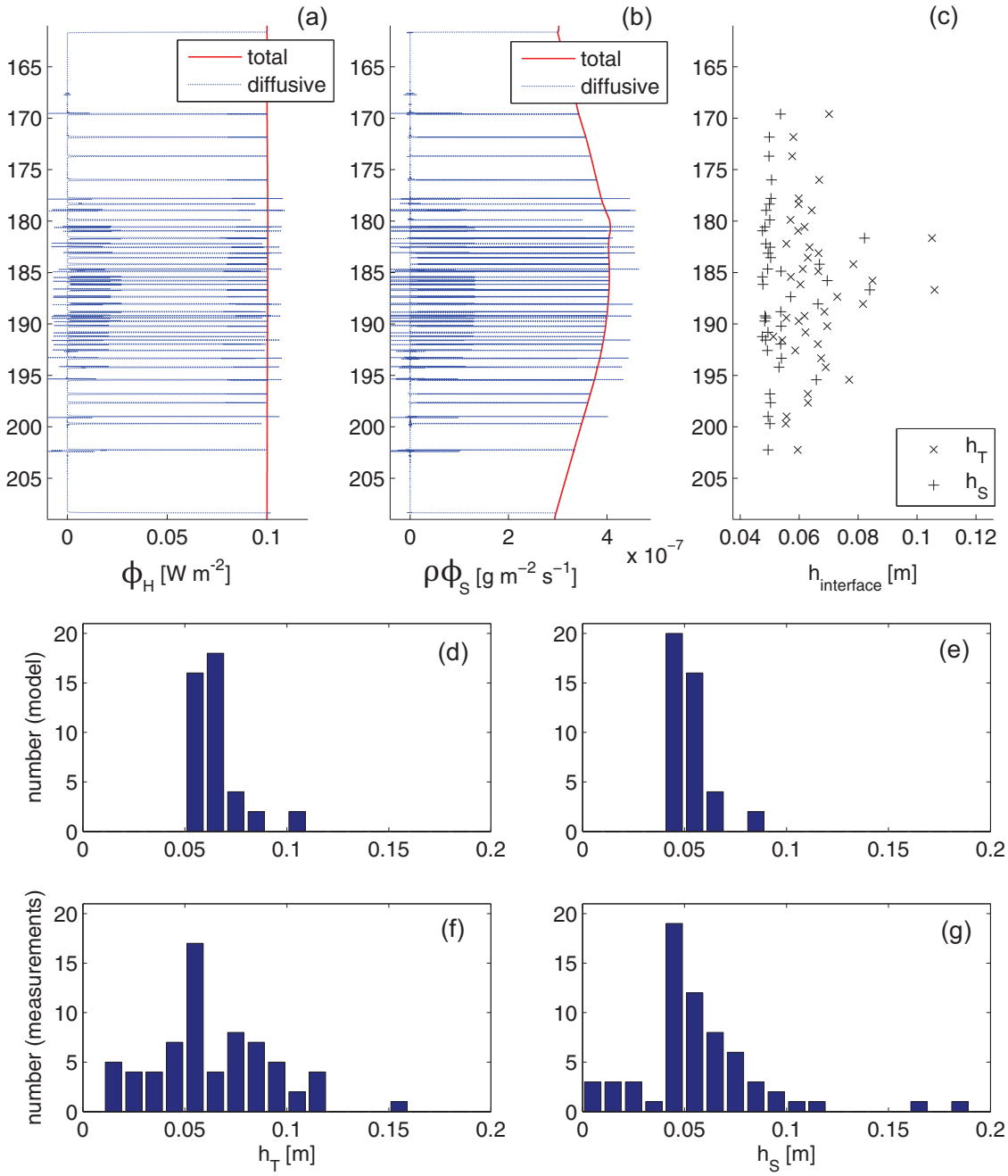

Figure 9. Vertical variation of the Lake Kivu results for (a) the heat flux ϕ_H; (b) the mass salt flux $\rho\phi_S$, distinguishing between the total flux and the diffusive component; and (c) interface thickness for temperature and salinity steps. The distributions of the interface thickness h_T and h_S are shown for both (d and e) model results and (f and g) measurements. The simulation is the same as in Figure 8.

epilimnion and are permanently stratified. Repeated profiles of *T* and *S* have been collected over a relatively long period [*Schmid et al.*, 2004], making it an interesting case for studying the evolution of a staircase structure. Lake Nyos is a peculiar case because the stability of the water column is due to large concentrations of CO_2, with *T* and *S* approximately balancing each other in the part of the water column that has been chosen to be simulated (between 52 and 100 m depth).

At the beginning of 2002 (first measurement on 23 March), cooling of the surface layer triggered the initiation of double diffusion and the subsequent formation of a staircase structure that propagated downward over the course of a few years. For the present analysis, we refer to three dates of the survey (*T* and *S*): 19

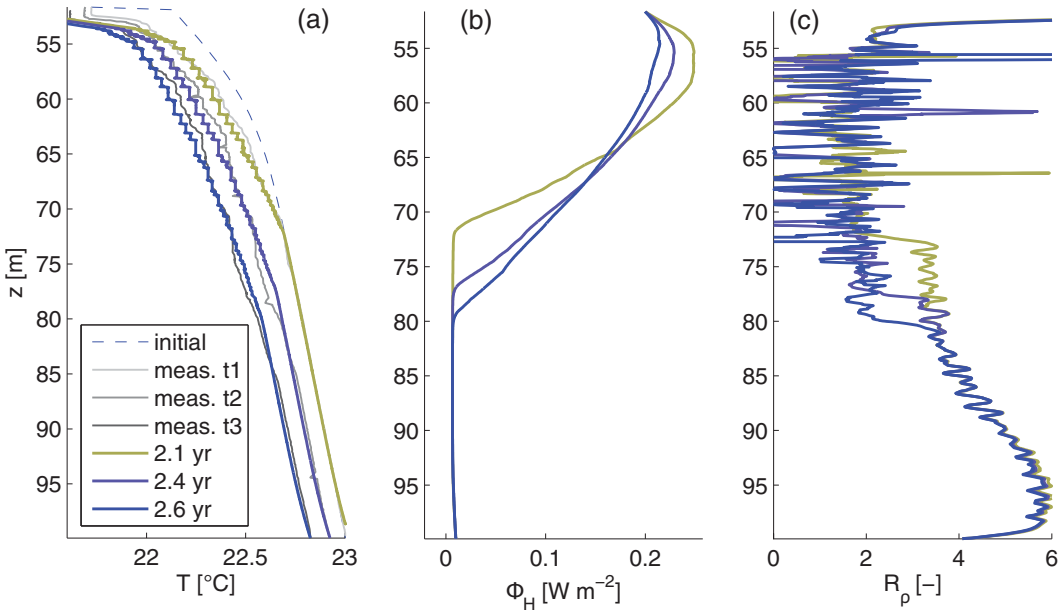

Figure 10. Double-diffusive staircase development in Lake Nyos: (a) comparison of temperature profiles at different times (the second and the third profiles are shifted by multiples of 0.1°C), measured on 19 July 2002 (t_1), 7 December 2002 (t_2), 9 January 2003 (t_3), and modeled at 2.1, 2.4, and 2.6 years (754, 873, and 952 days, respectively); (b) total heat flux ϕ_H; (c) vertical variation of the density ratio R_ρ (smoothed, negative values are due to temporary instabilities at the interfaces originated after the computational phase of sorting). Model parameters are reported in Table 1.

July and 7 December 2002, and 9 January 2003. The first profile shows only the initial phase of the formation of the staircase, while the second and third profiles clearly suggest that the double-diffusive structure rapidly expanded. Unfortunately, corresponding data of CO_2 concentration are not available, and only one profile was measured in January 2003 [*Kusakabe et al.*, 2008]. Such a profile has been used as a reference to define an equivalent salinity $S_e = S + (\beta_{CO_2}/\beta)\, C_{CO_2}$, where C_{CO_2} is the CO_2 concentration and β_{CO_2} its contraction coefficient (see Table 1).

The cooling effect is reproduced in the model by imposing a heat flux $\phi_H = 200$ mW m^{-2} at the upper boundary (calculated on the basis of the local temperature gradient) while keeping the background value (10 mW m^{-2}) at the lower boundary. The initial conditions have been imposed ~2 years before the first available measurement because the initial state and the perturbation triggering double diffusion are not known exactly. The initial temperature profile has been reconstructed by arbitrarily increasing T (with respect to the first survey) at the top, thus reducing its slope (see Figure 10a). The initial profile for the equivalent salinity S_e has been imposed by setting two analytical functions that approximate the available measurements of S and CO_2. The boundary conditions have been applied imposing the fluxes calculated using the local gradients of S_e at the top and at the bottom ($\rho\, \Phi_{S_e} = 3\times10^{-6}$ and 3×10^{-8} g m^{-2} s^{-1}, respectively).

The analysis of the formation, and downward propagation, of the staircase structure is focused on the temperature dynamics, for which more reliable data are available, while the lack of measurements yields uncertainties in the definition of the equivalent salinity. Figure 10a shows the comparison of the modeled evolution with the measurements (note that the second and third profiles are shifted leftward to allow for a clearer reading of the plots). The quantitative agreement is reasonable, given also the impact of the reconstructed S_e profile on some local features, such as medium-scale slope variability.

More interesting is that the model is able to reproduce the correct overall dynamics: (i) the onset of double diffusion triggered by the local instability produced by the cooling and (ii) the downward propagation of the front of the staircase, which creates new steps while the old ones remain approximately at the same position (consistent with observations by *Schmid et al.* [2004]). The dynamics are clearly visible in the

vertical shift of the excess heat flux generated by double diffusion (Figure 10b), which initially produces a maximum in the range of $z=$ 55–60 m (at 2.1 year), and then spreads out toward reaching a balance with the upper boundary condition. Interestingly, the formation of new steps at the lower boundary of the double-diffusive region results in a change of the density ratio R_ρ, which abruptly decreases to values oscillating around $\sim$2 (Figure 10c).

The strong variation of the fluxes along the vertical (Figure 10b) does not allow to define a value of λ_T a priori as in the previous two cases, which were approximately in steady state with a uniform heat flux. This is also confirmed by the fact that the selection of the best set of parameters (dz and λ_T, see Table 1) is less clear than in the other cases, so that the model outputs are relatively insensitive to the chosen values. Moreover, the model in this case is not able to reproduce the details of the staircase structure. Nevertheless, it captures the overall dynamics, suggesting the possibility to use such a simplified approach also in conditions that are far from steady state.

5. Discussion

5.1. On the Choice of the Parameters

The two parameters of the model, namely the water parcel size dz and the dimensionless time step parameter λ_T, fully characterize the internal mechanisms. The parameter dz is not crucial for the shape of the profiles of the variables (T and S), as discussed in section 3.3. It plays a role for the interface thickness and is also the scale of all relevant lengths. Since most of the quantities involved in the process depend on dimensionless ratios that do not contain an explicit influence of dz, its effect becomes less important while looking at the overall dynamics.

The second parameter, λ_T, is the factor controlling the slope of the temperature profile in the staircase structure, as noted in the discussion of equation (27) and explicitly shown in Figure 5. The parameter λ_T is associated with the unstable volume that has to be reached before triggering a buoyancy driven convective motion. In section 3.2, we have discussed a way to relate λ_T to the critical Rayleigh number that characterizes the breakdown of the boundary layer. The analysis of its impact on the large-scale profiles (section 3.3) suggests a dependence of the step temperature difference and of the heat flux on this parameter, which implies that λ_T cannot be chosen independently of the boundary conditions that impose the external heat flux.

The calibration of the model to the three lakes showed the need to adopt different values of λ_T. In those cases that are known to be in an approximate steady state (Powell Lake and Lake Kivu), the values of λ_T are consistent with the theoretical considerations developed in section 3.2, thus supporting the validity of the conceptual framework. This was not possible for Lake Nyos due to the marked unsteadiness and the large variation of the heat flux within a few meters of the forming staircase; nevertheless, the calibrated λ_T fell within the range of values obtained for the other two lakes.

As a final note, the initial condition assumed for the salinity profile directly influences the evolution of the temperature profile. In fact, being the transport of salt much weaker, the initial slope of S is maintained for a long time while T adapts to the external conditions by changing the staircase slope and step height, causing a change of R_ρ and hence of the stability of the structure.

5.2. The Claim for Simplicity and the Limits of the Model

The proposed model is likely the simplest model that can reproduce the typical structures arising in the diffusive regime of double-diffusive convection because it contains only the two fundamental processes (diffusion, convective stabilization). Without the need to introduce ad hoc formulations to generate the layering, complex structures spontaneously arise from local instabilities through a process of self-organization, in a way that is similar to other natural processes [e.g., *Feltz et al.*, 2006].

The model can be used to understand the general dynamics but cannot be an exact description of the details of the process. It completely lacks the small-scale dynamics of the interface evolution at substep description (both in time and space), and therefore depends on the calibration of some parameters. Moreover, the model parameters appear to be flux dependent, thus requiring a careful estimate in the unsteady case and when no measured data are available. One of the major advantages is that the model allows to

explicitly consider the effect of boundary conditions. Thus, instead of looking at single elements (the step of the staircase structure) or at schematic configurations, the proposed model aims at giving a complementary picture of the phenomenon, trying to assess how changes in the large-scale features (or over long time periods) can modify the double-diffusive structures.

Finally, it is worth noting that the formulation of the model is general and not limited to lakes. It can potentially be applied to any context where double diffusion is a relevant process, for instance in oceans, oil reservoirs and star interiors.

5.3. Possible Applications and Future Research

In this paper, the model has been formulated and applied to three case studies to discuss its characteristics and show its performances. Future research will be focused on testing the model along two directions, characterized by an effort toward verification and exploration, respectively.

As a first direction, a deeper analysis is required about the agreement (or contradiction) between the model results and the indications available from previous literature, in particular concerning the influence of the heat flux on the height and stability of the staircase steps. With reference to commonly used flux laws, like that proposed by *Kelley* [1990], the exponent (whether or not equal to 4/3) and the proportionality coefficient $C(R_\rho)$ (using Kelley's notation) could be determined from the overall dynamics and compared with empirical and theoretical findings.

A fundamental question concerns the range of possible R_ρ for staircase formation. The literature reports several cases with up to $R_\rho = 10$ [e.g., *Newell*, 1984], while a lower limit of 1.5–1.7 has been proposed [*Taylor*, 1988; *Kelley et al.*, 2003; *Radko et al.*, 2014b]. The simplicity of the model and the possibility to run a large number of simulations can be exploited to systematically investigate the limiting cases, referring to real large-scale profiles observed in the field or in laboratory, and to the results of stability analyses [*Carpenter et al.*, 2012b].

Along the same direction, the model can be tested against the results of more complex numerical tools (e.g., DNS) to explore the mechanism of layer formation and merging: preliminary results suggest that the simple one-dimensional dynamics qualitatively corresponds to the "interface vanishing mode" discussed in *Noguchi and Niino* [2010b] but not to the "layer vanishing mode." Moreover, differently from the results of their model, which evolves to a single large step that occupies the entire domain [*Noguchi and Niino*, 2010a], the present analysis suggests that the final state may be characterized by a number of steps. The implications on the long-term dynamics and the consistency with real observations are worth of being explored.

The second direction is characterized by the use of the model in problems of diffusive convection and staircases evolution to gain more physical insights. An uncommon feature of the model is the possibility to observe changes of the background gradients when staircases form. Moreover, the role of boundary conditions on the mechanisms of layer formation and evolution can be explored, and specifically in contexts where the boundary conditions evolve in time. These characteristics, associated with the possibility to include local disturbances (like intrusions) in the model, may allow for more realistic representations of natural conditions. Turbulent diffusivity could be incorporated, as well, to investigate the role of background disturbance on the occurrence of staircases. In fact, in deep and undisturbed lakes (such as Powell Lake), the layering is very pronounced, while in other systems staircases do not form probably because the environment is too turbulent (e.g., in the boundary region of Lake Kivu). Finally, statistical analyses on layer and interface dynamics can be performed to explore the variability of the process in different environments, where other interesting large data sets could be used such as the Arctic microstructure data [*Padman and Dillon*, 1987; *Dillon and Padman*, 1989].

6. Conclusions

In this study, we have formulated a simple one-dimensional model that is able to reproduce the main features of the typical large-scale structures of double-diffusive convection in the diffusive regime. The model is based on the identification of the two fundamental mechanisms acting on this process: molecular

diffusion in the stable regions, and convective transport in the well-mixed layers dominated by the buoyant volumes of gravitationally unstable water.

The model is defined by two parameters, the size of the basic elements of the discretized domain, dz, and the dimensionless time step considered for the solution of the heat diffusion equation, λ_T, which is a proxy for the definition of a threshold for the instability that produces the convective transport. The simplicity of the model allows for large-scale, long-term simulations, which can consider the effect of the boundary conditions. In this respect, the proposed approach suggests a change of perspective in the analysis of double-diffusive systems, shifting the focus from small-scale processes to the overall dynamics. The main drawback is that the two parameters of the model (and in particular λ_T) need calibration and can vary with the examined case. We are aware that the model cannot describe detailed processes that are not included in its formulation, like the short-term behavior or the small-scale structure of the diffusive interface. However, these inherent limits should not be considered as deficiencies but more as intrinsic restrictions.

The model has been analyzed from a theoretical point of view and tested in three different lakes (Powell, Kivu, and Nyos), always showing a satisfactory or even excellent agreement with the available measurements. Interestingly, the proposed approach suggests that double diffusion can be seen as a self-organizing process, another example of how extremely basic mechanisms produce, by means of a chain reaction dominated by a chaotic behavior, beautiful and simple structures like the staircase layering.

Appendix A: Numerical Solution

The diffusion equation is discretized using finite differences and solved numerically with an implicit centered numerical scheme. Considering the equation for the temperature:

$$\frac{T_i^{(k+1)}-T_i^{(k)}}{dt}=\kappa_T\frac{T_{i+1}^{(k+1)}-2T_i^{(k+1)}+T_{i-1}^{(k+1)}}{dz^2}\,, \tag{A1}$$

where i is the grid point and k the time index, the resulting numerical scheme is

$$(1+2\lambda_T)T_i^{(k+1)}-\lambda_T T_{i+1}^{(k+1)}-\lambda_T T_{i-1}^{(k+1)}=T_i^{(k)}\,, \tag{A2}$$

where λ_T is the diffusion parameter introduced in the main text by equation (11).

An identical approach is used for the salinity:

$$(1+2\lambda_S)S_i^{(k+1)}-\lambda_S S_{i+1}^{(k+1)}-\lambda_S S_{i-1}^{(k+1)}=S_i^{(k)}\,, \tag{A3}$$

for which the diffusion parameter

$$\lambda_S=\frac{\kappa_S\,dt}{dz^2}=\tau\,\lambda_T \tag{A4}$$

is always smaller than λ_T, given the proportionality coefficient $\tau \ll 1$. This implies that the numerical solution of the salinity equation is always correct if the equation for temperature is solved adequately.

The boundary conditions are applied at the lower computational point ($z_0=0$) and at the upper one ($z_n=L$). Fixed values of temperature and salinity can be prescribed through a Dirichlet boundary condition: $T_0=T_{bc1}$, $T_n=T_{bc2}$; $S_0=S_{bc1}$, $S_n=S_{bc2}$. Another possibility is to prescribed the fluxes of the two quantities by means of a Neumann condition: $\phi_{T,0}=\phi_{T,bc1}$, $\phi_{T,n-1}=\phi_{T,bc2}$; $\phi_{S,0}=\phi_{S,bc1}$, $\phi_{S,n-1}=\phi_{S,bc2}$. The fluxes are discretized in the following form:

$$T_1-T_2=\phi_{T,bc1}\frac{dz}{\kappa_T}\,,\qquad T_{n-1}-T_n=\phi_{T,bc2}\frac{dz}{\kappa_T}\,, \tag{A5}$$

$$S_1-S_2=\phi_{S,bc1}\frac{dz}{\kappa_S}\,,\qquad S_{n-1}-S_n=\phi_{T,bc2}\frac{dz}{\kappa_S}\,. \tag{A6}$$

The thermophysical water properties have been numerically evaluated using the freely available "CSIRO MatLAB Seawater Library" by Phil Morgan, CMR.

Appendix B: Steady State Profiles

B1. Dimensionless Formulation

In order to simplify the analysis, we express all quantities in dimensionless form (hereafter denoted by *) introducing the following scaling:

$$T^* = \frac{T - T_r}{\Delta T'}, \quad S^* = \frac{S - S_r}{\Delta S'}, \quad \rho^* = \frac{\rho - \rho_r}{\rho_r \alpha^*}, \qquad \alpha^* = \alpha \Delta T', \quad \beta^* = \beta \Delta S', \tag{B1}$$

where T_r, S_r, and ρ_r are locally defined as the central values of temperature, salinity, and density, respectively. The equation of state (3) is rewritten in dimensionless form to allow for simpler algebraic manipulation as follows:

$$\rho^* = -T^* + R'_\rho S^*, \qquad R'_\rho = \frac{\beta^*}{\alpha^*}. \tag{B2}$$

The dimensionless fluxes are defined with reference to the purely diffusive fluxes as follows:

$$\phi_T^* = \frac{H'}{\kappa_T \Delta T'} \phi_T, \qquad \phi_S^* = \frac{H'}{\kappa_S \Delta S'} \phi_S. \tag{B3}$$

The diffusion equations (1) are written in dimensionless form by considering suitable temporal and spatial scales. Referring to step height H' as a spatial scale, we can define the temporal scale $t'_T = H'^2/\kappa_T$ associated with the process of temperature diffusion. Hence, the dimensionless variables $z^* = z/H'$ and $t^* = t/t'_T$ can be introduced to give

$$\frac{\partial T^*}{\partial t^*} = \frac{\partial^2 T^*}{\partial z^{*2}}, \qquad \frac{\partial S^*}{\partial t^*} = \tau \frac{\partial^2 S^*}{\partial z^{*2}}. \tag{B4}$$

The governing equations (B4) can be discretized dividing the step height in $n'+1$ grid points, so that the dimensionless vertical spacing is $dz^* = 1/n'$. Using the time scale t'_T defined above, it follows that $\lambda_T = dt^*/dz^{*2}$ and $\lambda_S = \tau \lambda_T$.

We now focus on the lower half-interface (around $z^* = 0$) and assume that a steady state has been reached as a result of the balance between the diffusive fluxes at the interface and the convective flux. Referring to Figure 3, the diffusive fluxes between $z^* = 0$ and $z^* = dz^*$ are

$$\phi_{T,diff}^* = \frac{T_0^* - T_1^*}{dz^*}, \qquad \phi_{S,diff}^* = \frac{S_0^* - S_1^*}{dz^*}, \tag{B5}$$

where $T_0^* = S_0^* = 1/2$ are the values at the interface $z^* = 0$, and the gradient is calculated after the solution of the diffusion equation, consistent with the adopted implicit scheme. The convective flux is mimicked by the Lagrangian resorting of the $2n_u$ unstable parcels (n_u on each side of the step) of size dz^*,

$$\phi_{T,conv}^* = 2\sum_{i=1}^{n_u} \frac{T_i^* \, dz^*}{dt^*} = 2\, m_T \, \frac{T_1^* \, dz^*}{dt^*}, \qquad \phi_{S,conv}^* = 2\sum_{i=1}^{n_u} \frac{S_i^* \, dz^*}{dt^*} = \frac{2\, m_S}{\tau} \frac{S_1^* \, dz^*}{dt^*}, \tag{B6}$$

where we introduce two dimensionless numbers $m_T \geq 1$ and $m_S \geq 1$ indicating the total "mass" of temperature and salinity, respectively, of the moving parcels, scaled with the "mass" of the first grid point.

B2. Quantification of the Unstable Region

The coefficient m_T that allows for the calculation of T_1^* can be determined by means of a continued fraction. Let us assume that the density distribution is well ordered, meaning that ρ_1^* is more negative (negative and larger in absolute value) than ρ_2^* (as in Figure 3 after the diffusion step). In this case, we can determine T_2^* imposing the same condition used for T_1^*. In this process, we introduce a recursive definition of m_{Ti} as the partial "mass" relative to the value T_i^*:

$$m_1 T_1^* = T_1^* + m_2 T_2^*, \quad m_2 T_2^* = T_2^* + m_3 T_3^*, \tag{B7}$$

and so on until the last unstable $i = n_u$ (see below for its estimation). For brevity, in (B7), we temporarily drop the subscript T from the variable m_i and indicate with m_1 ($=m_T$) the "mass" calculated

in the first point, m_2 the value calculated in the second point, and accordingly for the following points.

The steady state balance between the diffusive and convective fluxes can be written as

$$\left(T_0^* - T_1^*\right)\lambda_T = 2m_1 T_1^* \,, \quad \left(T_1^* - T_2^*\right)\lambda_T = 2m_2 T_2^* \,, \tag{B8}$$

where $T_0^* = 1/2$. In general form, this reads

$$\left(T_{i-1}^* - T_i^*\right)\lambda_T = 2m_i T_i^* \,, \tag{B9}$$

from which the temperature can be reconstructed moving from the interface to the interior of the layer:

$$T_i^* = T_{i-1}^* \frac{\lambda_T}{2m_i + \lambda_T} \,. \tag{B10}$$

Recalling from equations (B7) that

$$m_{i-1} T_{i-1}^* = T_{i-1}^* + m_i T_i^* = T_{i-1}^* \left(1 + m_i \frac{\lambda_T}{2m_i + \lambda_T}\right) , \tag{B11}$$

a general continued fraction can be obtained in the form

$$m_i = 1 + \frac{m_{i+1}\,\lambda_T}{2m_{i+1} + \lambda_T} \,. \tag{B12}$$

The problem in the computation of m_1 is that it depends on the other points. This can be solved as follows: the maximum value of i, which denotes the last parcel which contributes to the total flux (i.e., negative ρ_i^* produced by T_i^* significantly different from 0) is related to the number of unstable parcels n_u. This number is estimated comparing the unstable length $n_u\,dz$ with the length scale of temperature diffusion $n_\sigma\sqrt{2\kappa_T\,dt}$. This implies that

$$n_u \simeq n_\sigma \sqrt{2\lambda_T} \,, \tag{B13}$$

where n_u is an integer and n_σ is a number that depends on the tolerance (e.g., $n_\sigma = 3$ indicates 99.8% of the total "mass"). Then, equation (B12) is used to calculate all values of m_i until we obtain $m_T = m_1$, and the relationship (B10) is used to calculate all values of T_i^* starting from $T_0^* = 1/2$ up to $T_{n_u}^*$. This algorithm provides the equilibrium profile for temperature.

An analogous derivation allows one to obtain the profile of salinity and the value of the coefficient m_S by using the two relationships

$$S_i^* = S_{i-1}^* \frac{\lambda_S}{2m_{Si} + \lambda_S} \,. \tag{B14}$$

$$m_{Si} = 1 + \frac{m_{Si+1}\,\lambda_S}{2m_{Si+1} + \lambda_S} \,. \tag{B15}$$

If $\tau \ll 1$ and λ_T is not too large, $\lambda_S \ll 1$ and hence $m_S \simeq 1$ and $S_1^* \simeq S_0^*\,\lambda_S/2 = \tau\,\lambda_T/4$.

By numerically comparing the results of the continuous fractions (B12) and (B15), it is possible to show that the equations (15) are valid.

Asking for stationary conditions requires that equations (B5) and (B6) are combined to obtain

$$\frac{T_0^* - T_1^*}{dz^*} = 2\,m_T \frac{T_1^*\,dz^*}{dt^*} \,, \quad \frac{S_0^* - S_1^*}{dz^*} = \frac{2\,m_S}{\tau}\frac{S_1^*\,dz^*}{dt^*} \,, \tag{B16}$$

from which the values of temperature and salinity at the first grid point can be estimated:

$$T_1^* = T_0^* \frac{\lambda_T}{2m_T + \lambda_T} \,, \qquad S_1^* = S_0^* \frac{\lambda_S}{2m_S + \lambda_S} \,. \tag{B17}$$

Now the fluxes can be easily calculated from (B5), yielding

$$\phi_T^* = \frac{T_0^*}{dz^*}\frac{2m_T}{2m_T+\lambda_T}\,, \qquad \phi_S^* = \frac{S_0^*}{dz^*}\frac{2m_S}{2m_S+\lambda_S}\,. \tag{B18}$$

Appendix C: Height and Stability of a Single Step

In this section, we propose a simplified estimate of height H' of a single step by means of the length scale of the diffusion process. We assume that if the latter exceeds half of the domain H', a separate convective zone does not exist. This condition can be cast in the same form as in equation (B13), i.e., $n_\sigma\sqrt{2\kappa_T dt} < H'/2$, which becomes $8n_\sigma^2\, dz^{*2}\,\lambda_T < 1$ in dimensionless terms. Considering the equality in this relationship to determine the height H', we can also write

$$H' = \zeta\,\lambda_T^{1/2}\,dz\,, \tag{C1}$$

where $\zeta = j\,2\sqrt{2}\,n_\sigma$, with $j \sim O(1)$. If we assume $n_\sigma = 3$ (see section B2), we obtain $\zeta \simeq 8.5\,j$. This suggests that the step height linearly depends on the size dz of the Lagrangian elements, which hence can be used as a scale for it, while it grows at a lower rate with λ_T.

Furthermore, we also consider the condition to have a stable step. The density difference produced by the diffusion in the first grid point,

$$\rho_1^* = -T_1^* + R'_\rho S_1^* = -\frac{\lambda_T/2}{2m_T+\lambda_T} + R'_\rho\frac{\lambda_S/2}{2m_S+\lambda_S}\,, \tag{C2}$$

has to be smaller in absolute value than the density difference at the upper interface $(-R_{\rho,s}+1)/2$ (see Figure 3) to have a stable step. Noting that both densities are negative, the condition can be written as $-\rho_1^* < (R_{\rho,s}-1)/2$. It follows that

$$\frac{\lambda_T}{2m_T+\lambda_T} - R'_\rho\frac{\lambda_S}{2m_S+\lambda_S} < R'_\rho - 1\,, \tag{C3}$$

$$\frac{2m_T+2\lambda_T}{2m_T+\lambda_T} < R'_\rho\,\frac{2m_S+2\lambda_S}{2m_S+\lambda_S} \simeq R'_\rho\,, \tag{C4}$$

where the last condition is approximately valid if $\lambda_S \ll 2m_S$. Since the ratio on the left-hand side is defined in the range 1–2, this condition is always satisfied if $R'_\rho > 2$. When R'_ρ tends to 1, λ_T has to be lower than a limit value in order to let the step exist.

Acknowledgments
This work has been developed during a period spent by the first author at EPFL—Ecole Polytechnique Fédérale de Lausanne, and supported by ENAC—Environmental Science and Engineering Section. The main ideas were however formulated during a research period spent at Eawag, Department of Surface Waters - Research and Management, where Marco Toffolon was supported by the project DEWAX, cofunded by Provincia Autonoma di Trento and European Commission (Marie Curie actions, project Trentino PCOFUND-GA-2008–226070, Researcher 2010 outgoing, Call 4). The source code of the model is available at https://github.com/marcotoffolon/minDD. A. Wüest will provide the data used in this work upon request. The authors thank Martin Schmid for the analysis of Lake Nyos results and insightful comments on the model, and Jeff Carpenter for fruitful discussions and useful comments on the manuscript.

References

Carpenter, J. R., and M.-L. Timmermans (2014), Does rotation influence double-diffusive fluxes in polar oceans?, *J. Phys. Oceanogr.*, *44*, 289–296, doi:10.1175/JPO-D-13-098.1.

Carpenter, J. R., T. Sommer, and A. Wüest (2012a), Simulations of a double-diffusive interface in the diffusive convection regime, *J. Fluid Mech.*, *711*, 411–436.

Carpenter, J. R., T. Sommer, and A. Wüest (2012b), Stability of a double-diffusive interface in the diffusive convection regime, *J. Phys. Oceanogr.*, *42*, 840–854, doi:10.1175/JPO-D-11-0118.1.

Descy, J.-P., F. Darchambeau, and M. Schmid (Eds.) (2012), *Lake Kivu: Limnology and Biogeochemistry of a Tropical Great Lake, Aquat. Ecol. Ser.*, *5*, Springer, Dordrecht, Netherlands, doi:10.1007/978-94-007-4243-7.

Dillon, T. M., and L. Padman (1989), Thermal microstructure and internal waves in the Canada Basin diffusive staircase, *Deep Sea Res., Part A*, *36*, 531–542.

Feltz, B., M. Crommelinck, and P. Goujon (2006), *Self-Organization and Emergence in Life Sciences*, pp. 1–360, Springer, Dordrecht, Netherlands, doi:10.1007/1-4020-3917-4.

Fernando, H. J. S. (1989), Buoyancy transfer across a diffusive interface, *J. Fluid Mech.*, *209*, 1–34, doi:10.1017/S0022112089003010.

Flanagan, J. D., A. S. Lefler, and T. Radko (2013), Heat transport through diffusive interfaces, *Geophys. Res. Lett.*, *40*, 2466–2470, doi:10.1002/grl.50440.

Fofonoff, N. P., and R. C. Millard (1983), Algorithms for computation of fundamental properties of seawater, *UNESCO Tech. Pap. Mar. Sci.*, *44*, 53.

Gonzalez-Juez, E., A. R. Kerstein, and D. O. Lignell (2011), Fluxes across double-diffusive interfaces: A one-dimensional-turbulence study, *J. Fluid Mech.*, *677*, 218–254, doi:10.1017/jfm.2011.78.

Huppert, H. E. (1971), On the stability of a series of double-diffusive layers, *Deep Sea Res. Oceanogr. Abstr.*, *18*, 1005–1021, doi:10.1016/0011–7471(71)90005-2.

Huppert, H. E., and J. S. Turner (1981), Double-diffusive convection, *J. Fluid Mech.*, *106*, 299–329.

Kelley, D. E. (1984), Effective diffusivities within oceanic thermohaline staircases, *J. Geophys. Res.*, *89*, 484–488.

Kelley, D. E. (1990), Fluxes through diffusive staircases: A new formulation, *J. Geophys. Res.*, *95*, 3365–3371, doi:10.1029/JC095iC03p03365.

Kelley, D. E., H. J. S. Fernando, A. E. Gargett, J. Tanny, and E. Özsoy (2003), The diffusive regime of double-diffusive convection, *Prog. Oceanogr.*, *56*, 461–468.

Kerstein, A. R. (1999), One-dimensional turbulence: Part 2. Staircases in double-diffusive convection, *Dyn. Atmos. Oceans*, *30*, 25–46.

Kusakabe, M., T. Ohba, Issa, Y. Yoshida, H. Satake, T. Ohizumi, W. C. Evans, G. Tanyileke, and G. W. Kling (2008), Evaluation of CO_2 in Lakes Monoun and Nyos, Camerun, before and during controlled degassing, *Geochem. J.*, *42*, 93–118.

Linden, P. F., and T. G. L. Shirtcliffe (1978), The diffusive interface in double-diffusive convection, *J. Fluid Mech.*, *87*, 417–432, doi:10.1017/S002211207800169X.

Marmorino, G., and D. Caldwell (1976), Heat and salt transport through a diffusive thermohaline interface, *Deep Sea Res. Oceanogr. Abstr.*, *23*, 59–67, doi:10.1016/0011-7471(76)90808-1.

Mirouh, G. M., P. Garaud, S. Stellmach, A. L. Traxler, and T. S. Wood (2012), A new model for mixing by double-diffusive convection (semi-convection): I. The conditions for layer formation, *Astrophys. J.*, *750*, 61, doi:10.1088/0004–637X/750/1/61.

Newell, T. (1984), Characteristics of double-diffusive interface at high density stability ratios, *J. Fluid Mech.*, *149*, 386–401, doi:10.1017/S0022112084002718.

Newman, F. C. (1976), Temperature steps in Lake Kivu: A bottom heated saline lake, *J. Phys. Oceanogr.*, *6*, 157–163.

Noguchi, T., and H. Niino (2010a), Multi-layered diffusive convection. Part 1. Spontaneous layer formation, *J. Fluid Mech.*, *651*, 443–464, doi:10.1017/S0022112009994150.

Noguchi, T., and H. Niino (2010b), Multi-layered diffusive convection. Part 2. Dynamics of layer evolution, *J. Fluid Mech.*, *651*, 465–481, doi:10.1017/S0022112010994160.

Osborn, T. R. (1973), Temperature microstructure in Powell Lake, *J. Phys. Oceanogr.*, *3*, 302–307, doi:10.1175/1520-0485(1973)003<0302:TMIPL>2.0.CO;2.

Padman, L., and T. M. Dillon (1987), Vertical heat fluxes through the Beaufort Sea thermohaline staircase, *J. Geophys. Res.*, *92*, 10,799–10,806.

Piccolroaz, S., and M. Toffolon (2013), Deep water renewal in Lake Baikal: A model for long-term analyses, *J. Geophys. Res.*, *118*, 6717–6733, doi:10.1002/2013JC009029.

Radko, T. (2003), A mechanism for layer formation in a double-diffusive fluid, *J. Fluid Mech.*, *497*, 365–380, doi:10.1017/S0022112003006785.

Radko, T. (2005), What determines the thickness of layers in a thermohaline staircase?, *J. Fluid Mech.*, *523*, 79–98, doi:10.1017/S0022112004002290.

Radko, T. (2007), Mechanics of merging events for a series of layers in a stratified turbulent fluid, *J. Fluid Mech.*, *577*, 251–273, doi:10.1017/S0022112007004703.

Radko, T. (2013), *Double-Diffusive Convection*, Cambridge Univ. Press, Cambridge, U. K.

Radko, T., J. D. Flanagan, S. Stellmach, and M.-L. Timmermans (2014a), Double-diffusive recipes. Part II: Layer-merging events, *J. Phys. Oceanogr.*, *44*(5), 1285–1305, doi:10.1175/JPO-D-13-0156.1.

Radko, T., A. Bulters, J. D. Flanagan, and J.-M. Campin (2014b), Double-diffusive recipes. Part I: Large-scale dynamics of thermohaline staircases, *J. Phys. Oceanogr.*, *44*(5), 1269–1284, doi:10.1175/JPO-D-13-0155.1.

Scheifele, B., R. Pawlowicz, T. Sommer, and A. Wüest (2014), Double diffusion in saline Powell Lake, British Columbia, *J. Phys. Oceanogr.*, *44*, 2893–2908, doi:10.1175/JPO-D-14-0070.1.

Schmid, M., A. Lorke, A. Wüest, M. Halbwachs, and G. Tanyileke (2003), Development and sensitivity analysis of a model for assessing stratification and safety of Lake Nyos during artificial degassing, *Ocean Dyn.*, *53*, 288–301, doi:10.1007/s10236-003-0032-0.

Schmid, M., A. Lorke, C. Dinkel, G. Tanyileke, and A. Wüest (2004), Double-diffusive convection in Lake Nyos, Cameroon, *Deep Sea Res., Part I*, *51*, 1097–1111, doi:10.1175/JPO-D-14-0070.1.

Schmid, M., M. Busbridge, and A. Wüest (2010), Double-diffusive convection in Lake Kivu, *Limnol. Oceanogr.*, *55*, 225–238.

Schmitt, R. W. (1994), Double diffusion in oceanography, *Annu. Rev. Fluid Mech.*, *26*, 255–285, doi:10.1146/annurev.fl.26.010194.001351.

Sommer, T., J. R. Carpenter, M. Schmid, R. G. Lueck, M. Schurter, and A. Wüest (2013), Interface structure and flux laws in a natural double-diffusive layering, *J. Geophys. Res.*, *118*, 6092–6106, doi:10.1002/2013JC009166.

Sommer, T., J. R. Carpenter, and A. Wüest (2014), Double-diffusive interfaces in Lake Kivu reproduced by direct numerical simulations, *Geophys. Res. Lett.*, *41*, 5114–5121, doi:10.1002/2014GL060716.

Taylor, J. (1988), The fluxes across a diffusive interface at low values of the density ratio, *Deep Sea Res., Part A*, *35*, 555–567.

Turner, J. S. (1965), The coupled turbulent transport of salt and heat across a sharp density interface, *Int. J. Heat Mass Transf.*, *8*, 759–767, doi:10.1016/0017–9310(65)90022-0.

Turner, J. S. (1974), Double-diffusive phenomena, *Annu. Rev. Fluid Mech.*, *6*, 37–54, doi:10.1146/annurev.fl.06.010174.000345.

Williams, P. M., W. H. Mathews, and G. L. Pickard (1961), A lake in British Columbia containing old sea-water, *Nature*, *191*, 830–832, doi:10.1038/191830b0.

Wood, T. S., P. Garaud, and S. Stellmach (2013), A new model for mixing by double-diffusive convection (semi-convection). II. The transport of heat and composition through layers, *Astrophys. J.*, *768*, 157, doi:10.1088/0004–637X/768/2/157.

Worster, M. G. (2004), Time-dependent fluxes across double-diffusive interfaces, *J. Fluid Mech.*, *505*, 287–307, doi:10.1017/S0022112004008523.

Wüest, A., G. Piepke, and J. D. Halfman (1996), Combined effects of dissolved solids and temperature on the density stratification of Lake Malawi (East Africa), in *The Limnology, Climatology and Paleoclimatology of the East African Lakes*, edited by T. C. Johnson and E. O. Odada, pp. 183–202, Gordon and Breach, N. Y.